

University of New Mexico
Undergraduate Honors Thesis

**Study of 3D and Low Gain Avalanche Detectors for Particle
Physics Experiments**

Author: Jordan Hernandez
Advisors: Sally Seidel and Jiahe Si



THE UNIVERSITY OF
NEW MEXICO.

Abstract

Qualities of state of the art silicon low gain avalanche detectors (LGADs) have been studied as a function of gamma dose. Precision timing and tracking detectors are an important element of experiments operating at the Large Hadron Collider (LHC) whose purpose is discovery of new physics and improved understanding of the Standard Model of particle physics. The Large Hadron Collider and its detectors will undergo upgrades in coming years that will enable them to observe increasingly rare processes which could be the key to discoveries. The upgrades entail development of new tracking detectors with excellent position resolution, excellent timing, and high tolerance to radiation damage. One such development is the recent innovation of AC-LGADs. Methods of characterizing qualities of these sensors have been developed. This includes the development of a method of directly measuring the bulk leakage current of these LGADs while excluding high guard ring current.

Contents

1	Introduction	3
1.1	The Particle Physics Context for Silicon Detectors	3
1.2	The LHC and the ATLAS Detector	3
1.3	Semiconductors	4
1.3.1	PN Junction	5
1.3.2	Depletion Voltage and Breakdown Voltage	7
1.3.3	Tracking Trajectories of Elementary Particles	9
1.4	Radiation	10
2	Sensors	12
2.1	3D sensors	12
2.2	LGAD sensors	13
3	Measurement Procedure	15
3.1	Operational Range	15
3.2	IV scans	15
3.3	CV scans	19
3.4	Environmental effects on measurements	22
4	Results	24
4.1	Introduction	24

4.2	3D sensors	25
4.3	LGADs	26
4.3.1	AC-LGADs	28
4.3.2	BNL DC-LGADs	31
5	Conclusion	34
6	Acknowledgment	35

Chapter 1

Introduction

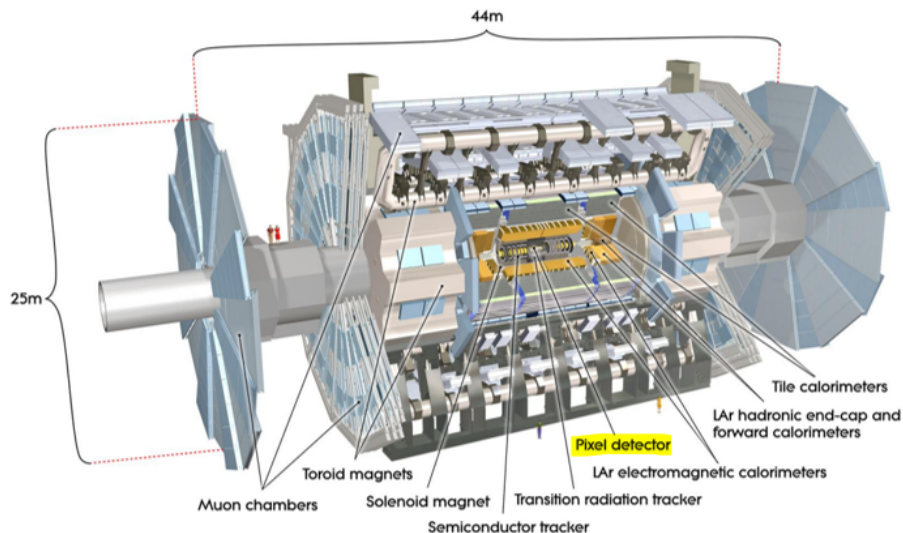
1.1 The Particle Physics Context for Silicon Detectors

Particle physics studies the most fundamental particles. These most fundamental particles are represented by the Standard Model. Fundamental particles are primarily characterized by their mass, charge, and spin. There are three known types of matter: quarks, leptons, and bosons (force carriers). Particle physics experiments often search for new physics beyond the Standard Model. One of the primary facilities for these searches is at Conseil Européen pour la Recherche Nucléaire (CERN) at the Large Hadron Collider (LHC).

1.2 The LHC and the ATLAS Detector

The LHC is the world's largest particle accelerator and is located near Geneva underground at CERN. There are 4 detectors on the LHC ring: ATLAS, ALICE, CMS, and LHCb. The ATLAS detector measures the

Figure 1.1: The ATLAS Detector at the LHC.



trajectories of charged particles produced in LHC collisions. The ATLAS detector is currently preparing to upgrade to explore new physics beyond the Standard Model. These upgrades will require new tracking technologies that are more radiation hard and able to provide timing measurements. The upgrades to the experiments at the collider may use the detectors described in this thesis in the next upgrade.

1.3 Semiconductors

The sensors described here are based on semiconductor technology. Semiconductors are materials with a conductivity between that of an insulator and a conductor. Typically, silicon is used for particle physics detectors. These detectors function by having a minimum ionizing particle, or MIP, pass through their PN junction. While doing so this MIP can interact with electrons in the valence shell of an atom and excite them to the conduction

band (Neaman, p. 619). This creates an electron hole pair that is then interpreted to provide information about the particle that passed through the detector.

1.3.1 PN Junction

The “p” in “pn junction” refers to a doped region within a semiconductor. This region includes acceptors. The “n” in pn junction is a doped region with donors. Fig. (1.2) illustrates a pn junction. Initially these two doped regions are electrically neutral, meaning the net charge on each side is 0. Then the junction is formed by bringing them into contact. Some of the electrons from the donors diffuse to the acceptors to occupy their valence shell. This results in a non-zero net charge in both regions, thus creating an electric field. To conduct experiments in a detection volume of macroscopic width, this electric field is then extended by applying a reverse bias voltage, see Fig. (1.3). This reverse bias voltage removes free charges, allowing information-carrying charges to be generated by ionization. The reverse bias applied to a sensor for particle physics experiments is within an operational range that is determined by the depletion voltage and breakdown voltage measurements described below.

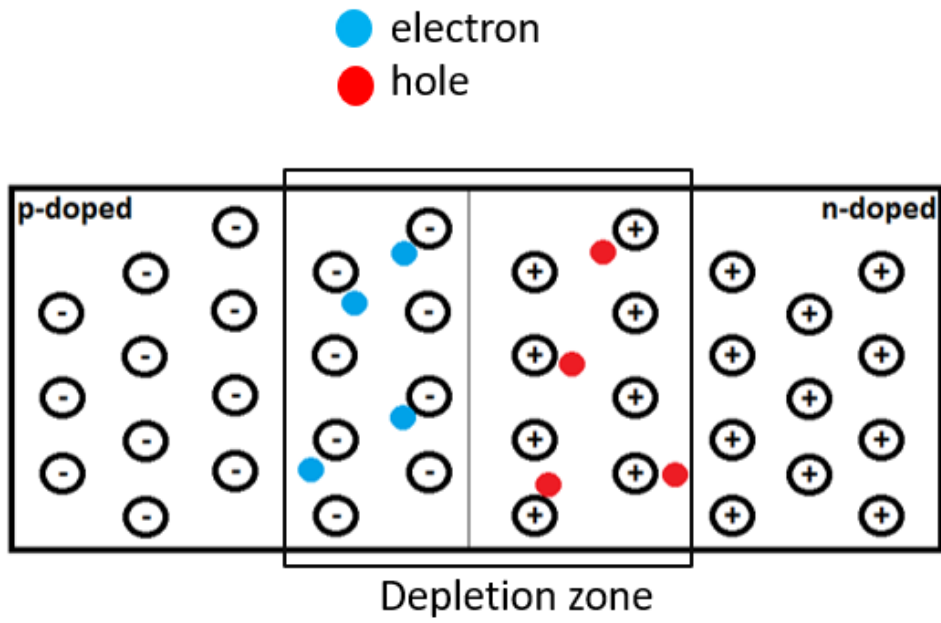


Figure 1.2: A p-n junction with free electrons and holes. This is before electrons fill valence shells.

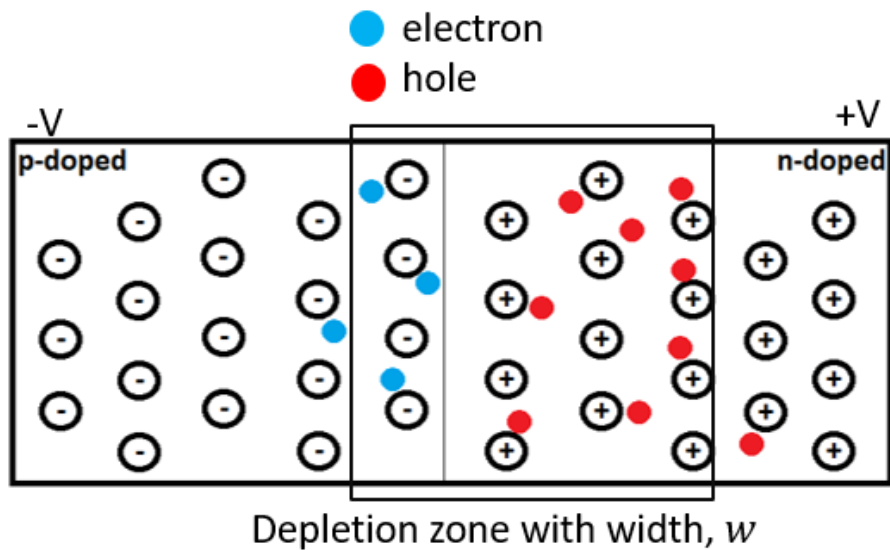


Figure 1.3: A p-n junction with reverse bias voltage applied. This results in an extended electric field beyond the p-n junction.

1.3.2 Depletion Voltage and Breakdown Voltage

The operational range of a sensor extends from the maximum voltage (given by the breakdown voltage) to the minimum voltage (given by the depletion voltage). As the reverse bias voltage is increased, more bulk silicon is depleted until the sensor is fully depleted. This voltage of full depletion is called the depletion voltage. The depletion voltage is found experimentally by measuring the bulk capacitance. A CV graph compares the bulk capacitance, C , to the bias voltage, V , of a sensor. The bulk capacitance is typically graphed as $\frac{1}{C^2}$ to make it easier to see where the depletion voltage occurs. Two best fit lines are then drawn and the point of intersection is identified as the depletion voltage, see Fig. (1.4).

The breakdown voltage is the voltage at which the semiconductor behaves

as a conductor. This can be seen by measuring the leakage current, I , of the sensor as a function of applied bias, V . The leakage current is often shown on an exponential scale to enhance where breakdown occurs, see Fig. (1.5).

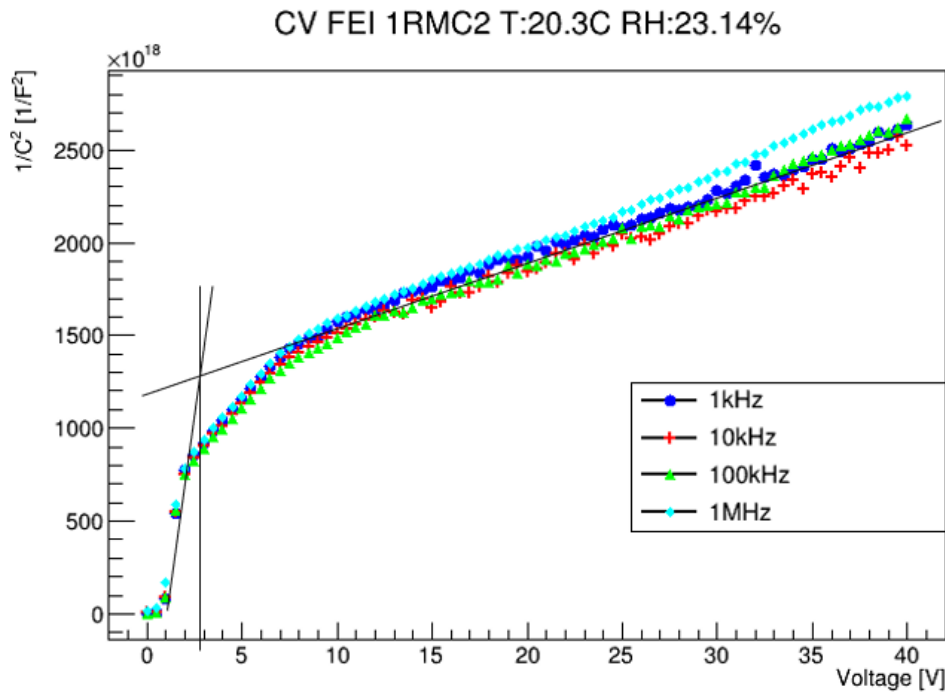


Figure 1.4: CV scan of sensor FEI 1RMC2 with best fit lines to show the method of determining depletion voltage. Four frequencies were used during measurements. The frequency 100kHz corresponded best to this sensor's bulk. Bottom-Right refers to the bottom right contact pad being used during this experiment, to identify which of this sensor's 4 contact pads were used.

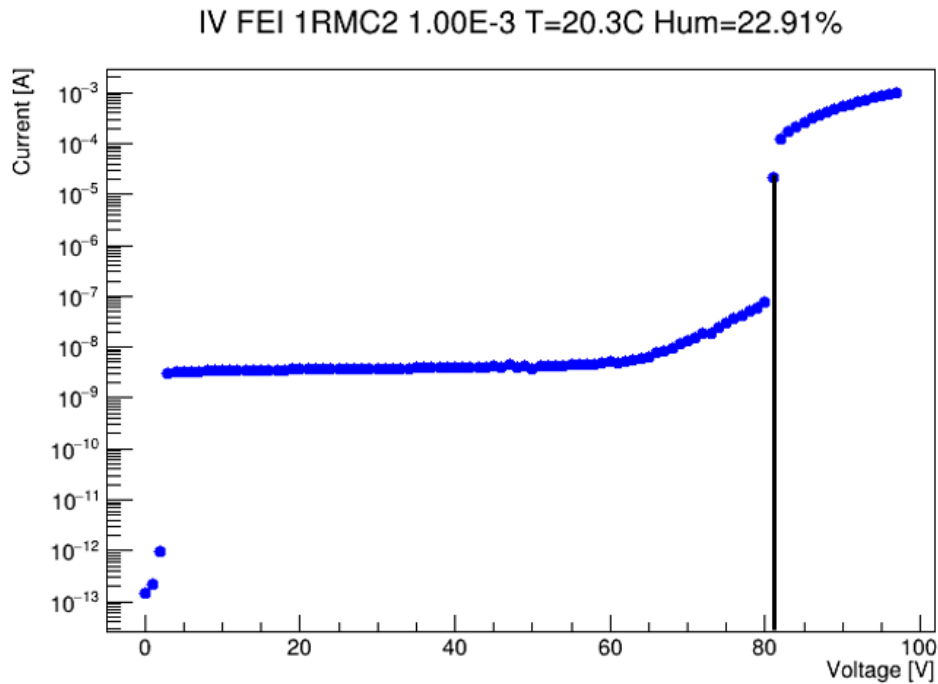


Figure 1.5: Bulk leakage current versus applied bias voltage of FEI 1RMC2 to show how the breakdown voltage is determined. The 1.00E-3 refers to the compliance current above which bias is not applied, to prevent damage to the sensor. The bottom right pad was used during this measurement.

It is important to record the humidity and temperature condition of the sensor during measurements as this can affect the operational range of a sensor (McDuff, p. 4). This is evident in measurements of the breakdown voltage of a sensor. As the temperature of a sensor increases, so does its breakdown voltage.

1.3.3 Tracking Trajectories of Elementary Particles

A minimum ionizing particle, or MIP, is a particle that when passing through the sensor creates electron hole pairs, as shown in Fig (1.6).

1.4 Radiation

Radiation refers to the emission of a particle from a source. The unit of radiation is the rad, short for radiation absorbed dose, and it indicates the energy absorbed. An object with 1 rad has absorbed 100 ergs (1 erg = 100 nJ) of energy for every 1 gram of mass that object has.

This paper studies the response of LGADs to gamma irradiation. “Gamma” refers to the energy that a photon, a type of boson, has. The sensors here were irradiated with Co-60 which produces gammas of energies 1.173 and 1.332 MeV. For LGADs in which the effects of irradiation were examined, 4 of each type of sensor (AC-LGAD pixel W3051, AC-LGAD strip W3073, and DC-LGAD W3045) received different radiation doses. This irradiation was conducted at the Sandia National Laboratories. One of each sensor was irradiated to 40 Mrad, 400 Mrad, or 1 Grad, and a control was retained unirradiated. After irradiation all sensors were placed in a freezer with a continuous temperature of -25°C to prevent annealing. Before measurement these sensors were placed in a room temperature bag filled N_2 to prevent condensation.

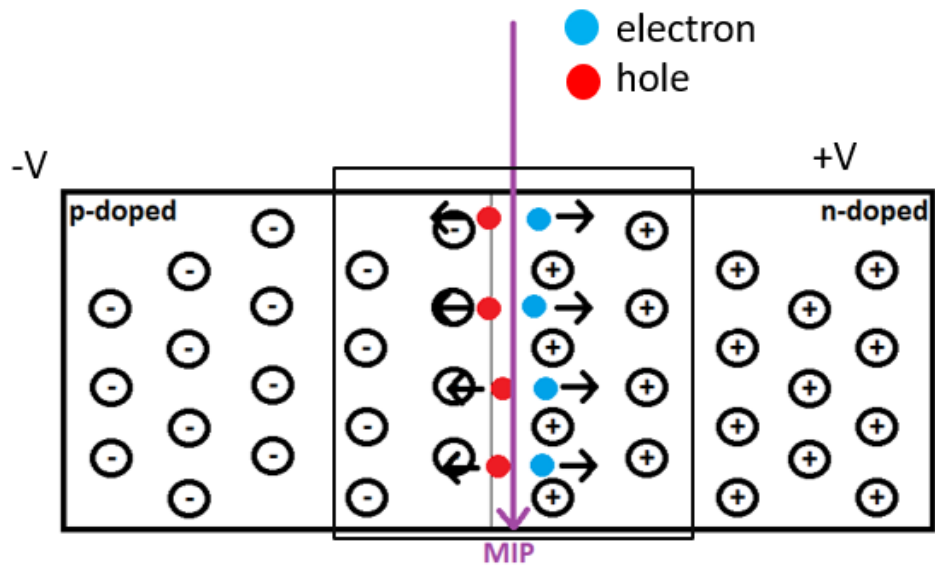


Figure 1.6: A p-n junction with incident MIP resulting in electron hole-pairs that electrically transmit information about the incident MIP.

Chapter 2

Sensors

The sensors reported here are 3D sensors and LGAD sensors. Both of these are silicon sensors whose design is motivated by the goals of excellent timing and position resolution, and radiation hardness. These are both state of the art detectors that may be implemented in the next LHC upgrade. The planar silicon sensor technology has electrodes arranged parallel to the wafer surface. 3D sensors have their electrodes implanted vertically. On a planar-type wafer, there is a surface n^+ region on which is fabricated the electrode and its contact pad of the sensor. The distance, w , between the front and back sides is typically $\approx 300\mu m$.

2.1 3D sensors

The technological benefits of 3D detectors (see Fig. 2.1) come from the vertical orientation of their electrodes in the bulk (Da Vià, p. 61). This allows the distance between electrodes to be much shorter than 300 microns. This allows 3D sensors to deplete the detection volume at a lower bias potential, than in the planar case. This structure also gives 3D sensors faster charge collection times, and it improves their radiation hardness, because

the charge collection distance can be less than the mean trapping distance.

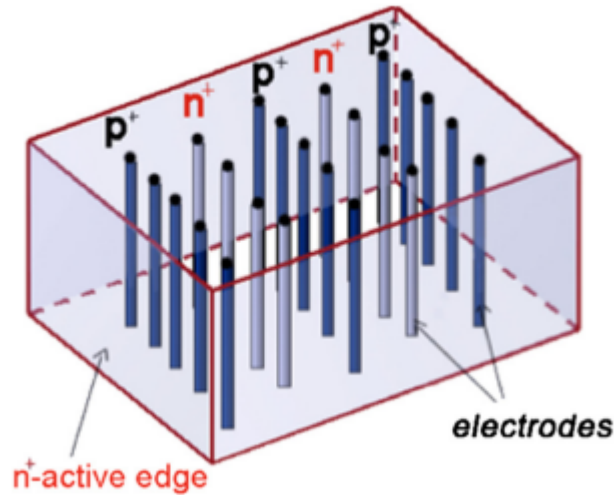


Figure 2.1: Sketch of a 3D detector where the p^+ and n^+ electrodes are inside the silicon bulk. The edges are p^+ electrodes (active edges) that surround the sides of the 3D device. [Obertino]

2.2 LGAD sensors

The technological benefits of an LGAD (Pellegrini, Sadrozinski) come from the inclusion of the gain layer, which multiplies signal. Multiple variations of LGADs have been developed. This report concerns LGADs of two types, DC-LGADs and AC-LGADs (Giacomini, 2019). What makes DC-LGADs different than conventional planar detectors is their high concentration p^+ layer, which is directly below the n^+ electrode. The p^+ layer creates a localized high electric field that multiplies electrons produced by MIPs. The sensor is very thin and this leads to precise time measurements (Ferrero, p. 16). The LGADs have a guard ring to insulate the bulk from external currents and structure the internal electric field so that it is uniform at the

active edge. The guard ring is located around the physical edge of a sensor (Ferrero, p. 33). AC-LGADs have no dead zones between electrodes. Fig. 2.2 shows the structure of a DC-LGAD and Fig. 2.3 shows the structure of an AC-LGAD.

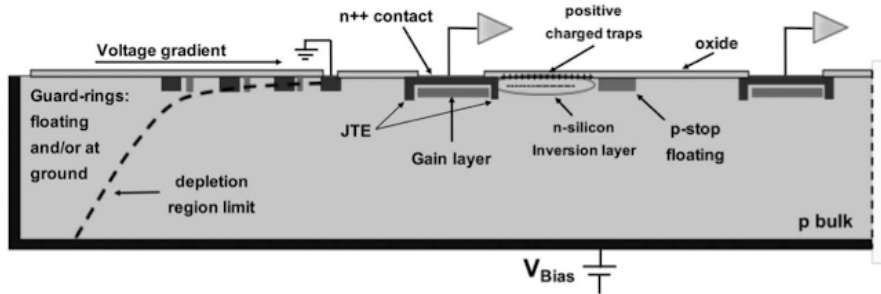


Figure 2.2: Cross cut of a multi-pad LGAD (not to scale) with a schematic view of the building blocks of the device. From the device physical edge: guard-rings, pad with JTEs, inter-pad region with p-stop. [Ferrero]

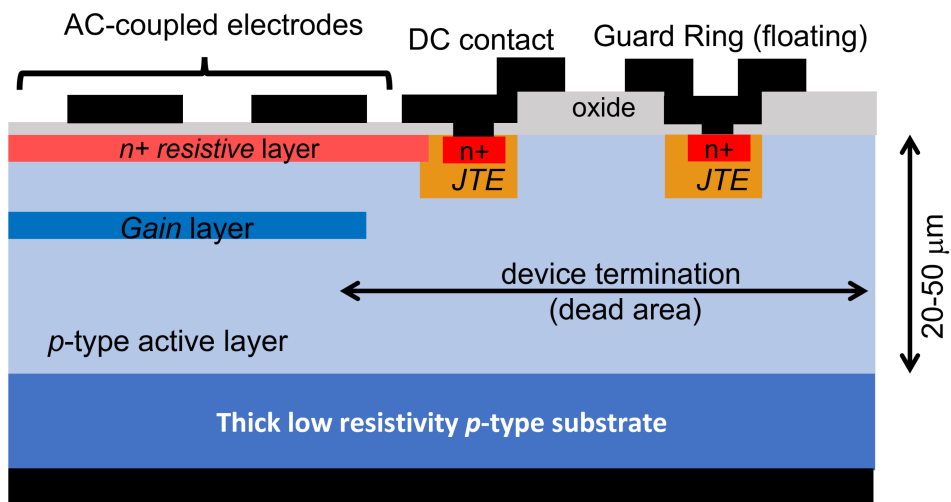


Figure 2.3: Sketch, not to scale, of a typical cross section of an AC-LGAD, showing the main components as described in the text. [Giacomini, 2023]

Chapter 3

Measurement Procedure

3.1 Operational Range

The operational range of a sensor is the range between the depletion voltage and the breakdown voltage. The breakdown voltage is the voltage at which one of two processes occurs, an avalanche effect or Zener effect (Neaman, p. 258). In the avalanche effect, charge carriers obtain a kinetic energy sufficient to excite additional charge carriers from the valence shell of atoms resulting in multiple free charges. This process which is most relevant to the study here, continues as voltage increases and results in an exponential increase of the bulk leakage current. For this reason just below breakdown is the maximum potential for the operational range of a sensor. The minimum potential for the operational range of a sensor is the depletion voltage.

3.2 IV scans

Measuring the leakage current allows us to find the breakdown voltage. The setup, shown in Figure (3.1), used for all IV scans on 3D sensors in this report, is called IV setup 1. LGADs require a different setup because the

guard ring must be connected to ground as shown in Figure 3.2. In this report it is also shown that different setups are used for different LGAD types.

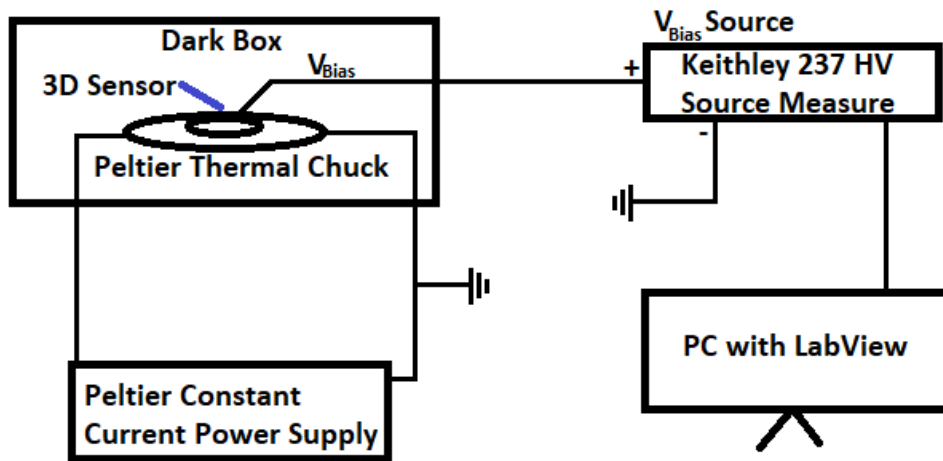


Figure 3.1: Setup for measuring the leakage current as a function of applied bias of a sensor. This is the setup that was used in measuring the leakage current for all 3D sensors in this report.

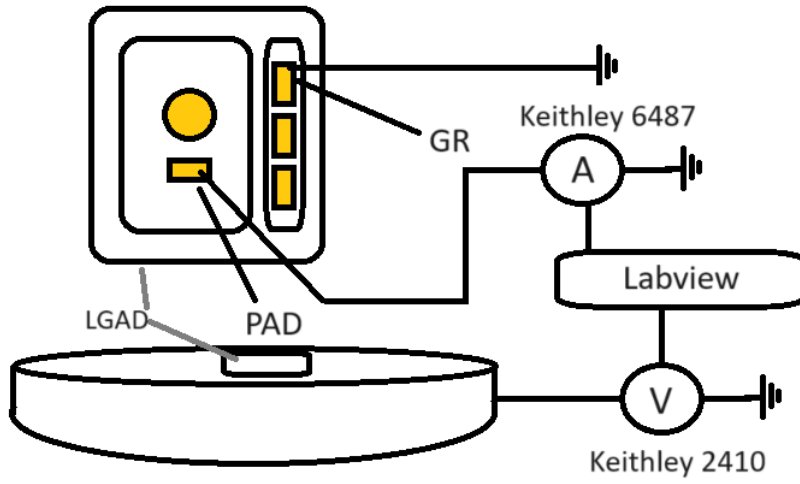


Figure 3.2: Setup for measuring the leakage current of a sensor with a guard ring as a function of applied bias. The guard ring is grounded. Here an ammeter is used to read the bulk current induced on the pad of the sensor.

To begin an IV measurement of the 3D sensors using the first setup, the Peltier thermal cooling system needs to be powered on and have cooling fans turned on. The cooling fans are located outside of the dark box and are used to cool down a liquid coolant within a radiator. This liquid coolant is used to remove heat from the hot side of the Peltier thermal chuck. A sensor is then removed from its protective tray using plastic forceps (metal ones could damage the sensor). The sensor is placed on a copper tray that is conductive. This copper tray holding the sensor is then placed on the Peltier thermal chuck. A probe connected to the sourcemeter, to measure leakage current, is then landed on the readout pad viewed through a microscope. A program written in LabVIEW is used to raise the applied bias voltage in steps. The maximum bias is set according to the expected breakdown voltage of the sensor. The LabVIEW program monitors the current to stop a measurement immediately when the compliance current is met. The current and voltage data are saved and interpreted via a program written in CERN's graphical programming language ROOT. Analysis of these data provides the breakdown voltage of a sensor.

The depletion voltage of the LGADs is determined by measuring the leakage current. The depletion voltage can not be observed by the first setup because the sourcemeter records the leakage current from both the pad and the guard ring. The guard ring current, for LGAD sensors being studied in this paper, is normally a few orders of magnitude higher than the pad current, until breakdown. So to find the depletion voltage of an LGAD sensor, an ammeter is used to directly measure the current through the pad. This is the motivation for creating a second setup for measuring IV. For Setup 2, the Peltier thermal chuck, Peltier constant current power supply and dark box are used as in the first setup shown in Figure (3.1).

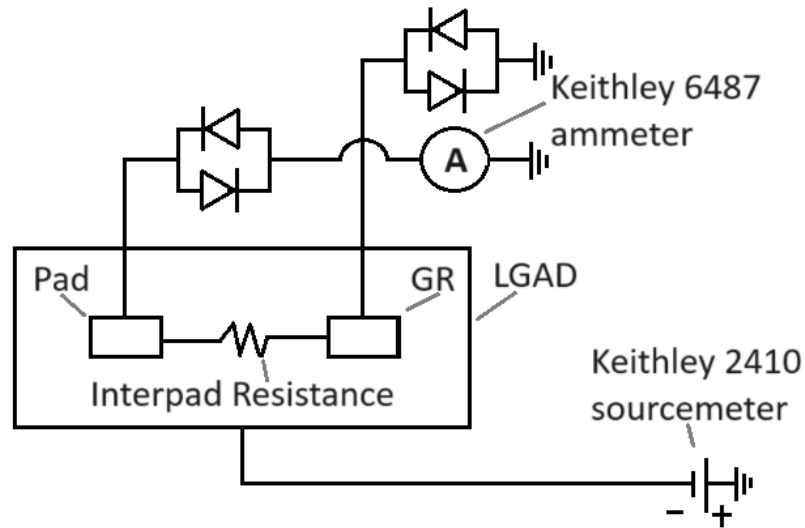


Figure 3.3: Second IV setup. Use of an ammeter to directly measure the current from the pad shown. This setup was the first where features could be observed for LGADs.

When conducting an IV measurement using the second setup the probe is now connected to the ammeter instead of the sourcemeter. So each step is followed as described above except now the probe on the pad is connected to the ammeter for measurement. The source meter is used to measure the total current (current from pad and guard ring). For sensors with a guard ring, this measurement checks that the guard ring is connected to ground as shown in Figure (3.3).

3.3 CV scans

CV scans are used to measure the bulk capacitance of a depleted sensor. Several frequencies are applied sequentially; this is done to find which frequency works best for the geometry of the structures being measured. For

LGADs the standard is 10kHz. The setup for doing this is the same for both LGAD and 3D sensors, as shown in Figure (3.4).

It was found that for some sensors the low interpad resistance required a modification to the bias isolation box. The structure of the bias isolation box is shown in Figure (3.5). For sensors of low internal resistance C2 had to increase in capacitance to $210\mu F$ instead of $1\mu F$. With this new capacitance, measurements showed features unobserved previously.

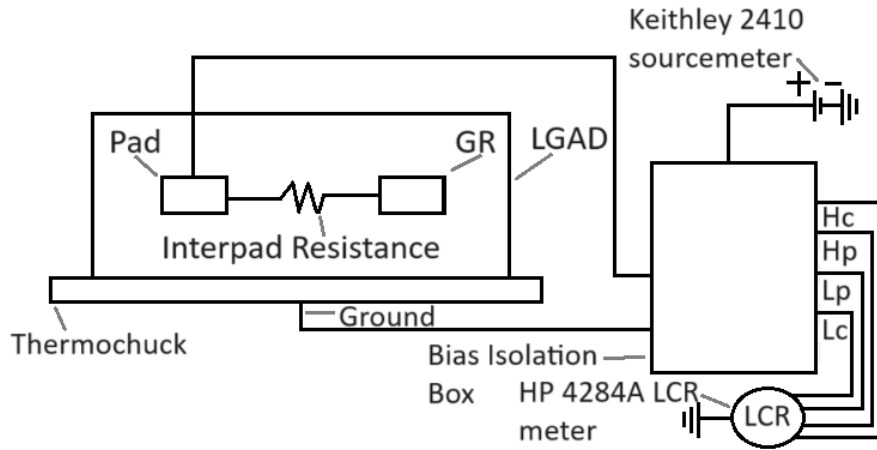


Figure 3.4: CV setup. This is the primary method for determining the depletion voltage of LGADs and 3D sensors.

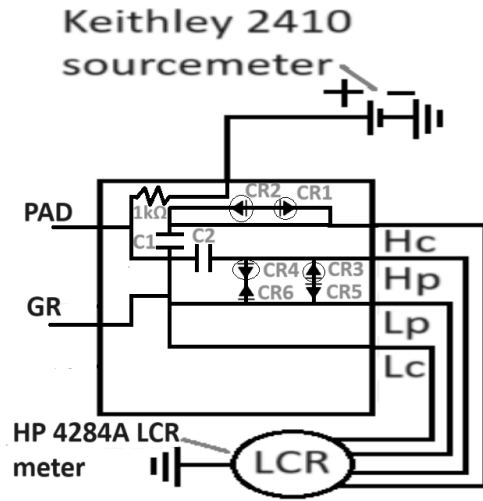


Figure 3.5: Bias isolation box. Here C2 is the capacitor which is changed as detailed in this paper.

Preparing a CV measurement is similar to that of an IV measurement. First the Peltier thermal cooling system needs to be powered on and have the cooling fans turned on, ensuring the temperature is regulated throughout the measurement. A sensor is then removed from its protective tray using plastic forceps. The sensor is placed on a copper tray and then moved to the thermal chuck. A probe connected to the bias isolation box, to measure bulk capacitance, is then placed above the readout pad of the sensor, without making contact. Then, the LCR meter conducts an open measurement for calibration. This done to account for the parallel parasitic impedance of the setup. After calibration the probe is lowered on to the pad. Then the applied DC voltage is gradually increased by the Keithley 2410 source meter Fig. (3.4), applied to the sensor through a $1k\Omega$ resistor, as shown on Figure

(3.5). The Keithley 2410 source meter is controlled by a LabVIEW program which also controls the HP 4284A LCR meter. Then the capacitance and voltage data are saved and sequentially studied via a ROOT program.

When measuring the capacitance of the sensor, the LabVIEW program treats the measured sensor as if it is a capacitor and resistor in parallel with each other. Using the LCR meter the parallel resistance can also be measured while conducting the CV measurement providing an RPV measurement. This RPV measurement might also provide an estimate of the depletion voltage.

3.4 Environmental effects on measurements

A rise in temperature increases the leakage current while also reducing the breakdown voltage of the sensor (S_{ze}), as shown in Fig. (3.6). The following equation converts leakage current of a sensor at temperature, T , to that at a temperature, T_R .

$$I(T_R) = I(T) \times \left(\frac{T_R}{T}\right)^3 e^{-\frac{E_{eff}}{2k_B} \left(\frac{1}{T_R} - \frac{1}{T}\right)} .$$

Here E_{eff} is the effective silicon band gap and k_B is the Boltzmann constant.

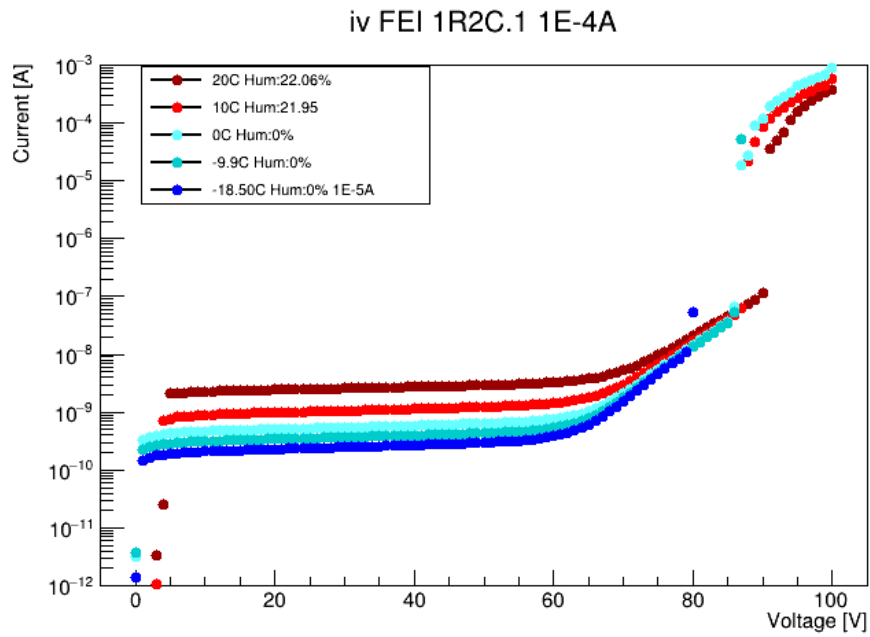


Figure 3.6: This is an IV graph of 3D sensor FEI 1R2C.1 taken at 5 different temperatures. Here the temperature can be seen to be directly affecting the leakage current and breakdown voltage of the sensor.

Chapter 4

Results

4.1 Introduction

This chapter concerns the measured leakage currents and depletion and breakdown voltages. Due to lack of time, a complete error analysis was not conducted. The uncertainties used are analogous to these reported in related papers describing measurements of similar devices conducted in the same laboratory. In these studies, the authors found that, “the errors on the IV and CV measurements include statistical and systematic uncertainties. Systematic uncertainties include uncertainties associated with the setup configuration (typically 1.9%), the accuracy of the source and measurement instruments ($\pm 0.3\% + 100$ fA for the Keithley 237; $\pm 0.029\% + 300$ pA for the Keithley 2410, and $\pm 0.34\%$ for the HP4284A), the precision of the measurement of the temperature ($\pm 0.5^\circ$ C leads to uncertainty of $\pm 1.82\%$ on leakage current)” (Hoferkamp). And, “The uncertainty in determining the voltage where the CV graph had an inflection point, which is related to the sampling frequency” (Sorenson, 7).

4.2 3D sensors

The operational range for 3D sensors was determined by estimating the depletion voltage by IV measurement, and by estimating the breakdown voltage by IV measurement. Figures 4.1 and 4.2 are example IV measurements on 3D sensors.

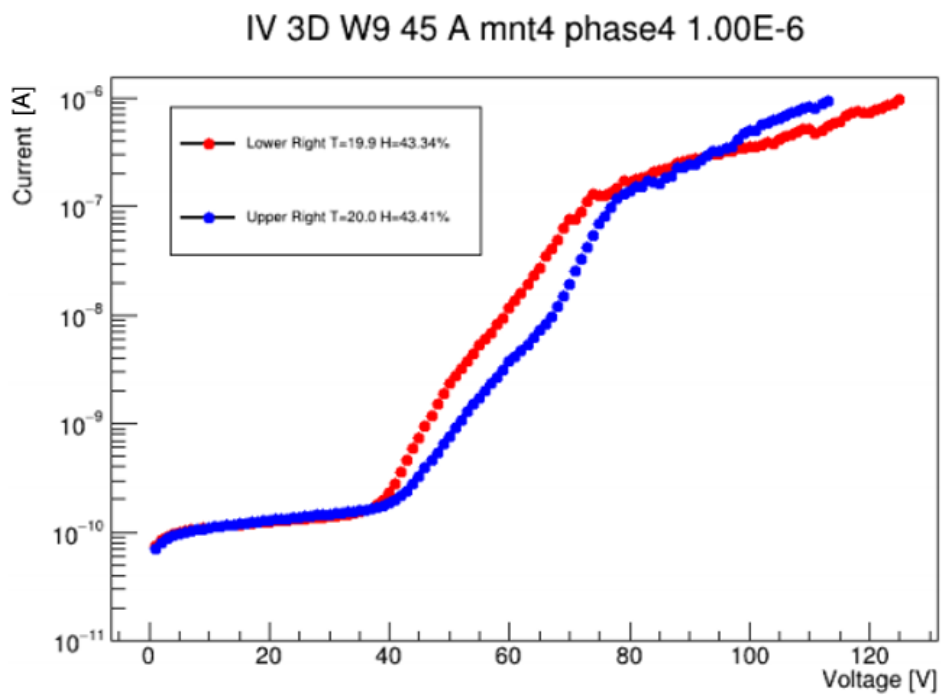


Figure 4.1: Standard IV measurement of the 3D sensor 201 W9 45 A

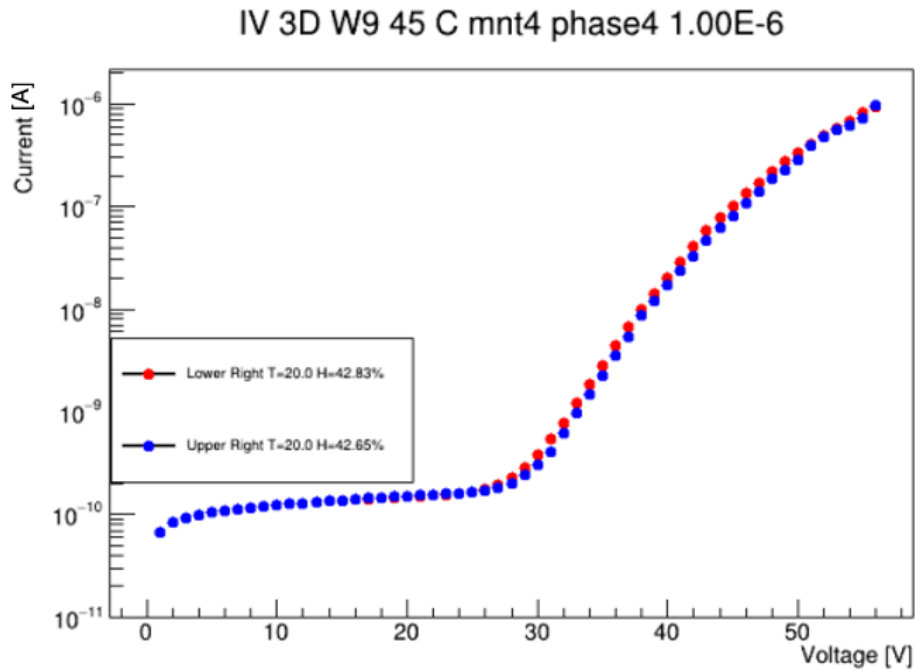


Figure 4.2: Standard IV measurement of the 3D sensor 201 W9 45 C

4.3 LGADs

The operational range for LGAD sensors was determined by estimating the depletion voltage by CV measurement, and by estimating the breakdown voltage by IV measurement. Figures 4.3, 4.4, and 4.5 show a comparison of characteristics of these sensors versus fluence from irradiation of these sensors. Figure 4.3 shows the gain layer depletion voltage versus fluence, and the full depletion voltage versus fluence for DC-LGADs.

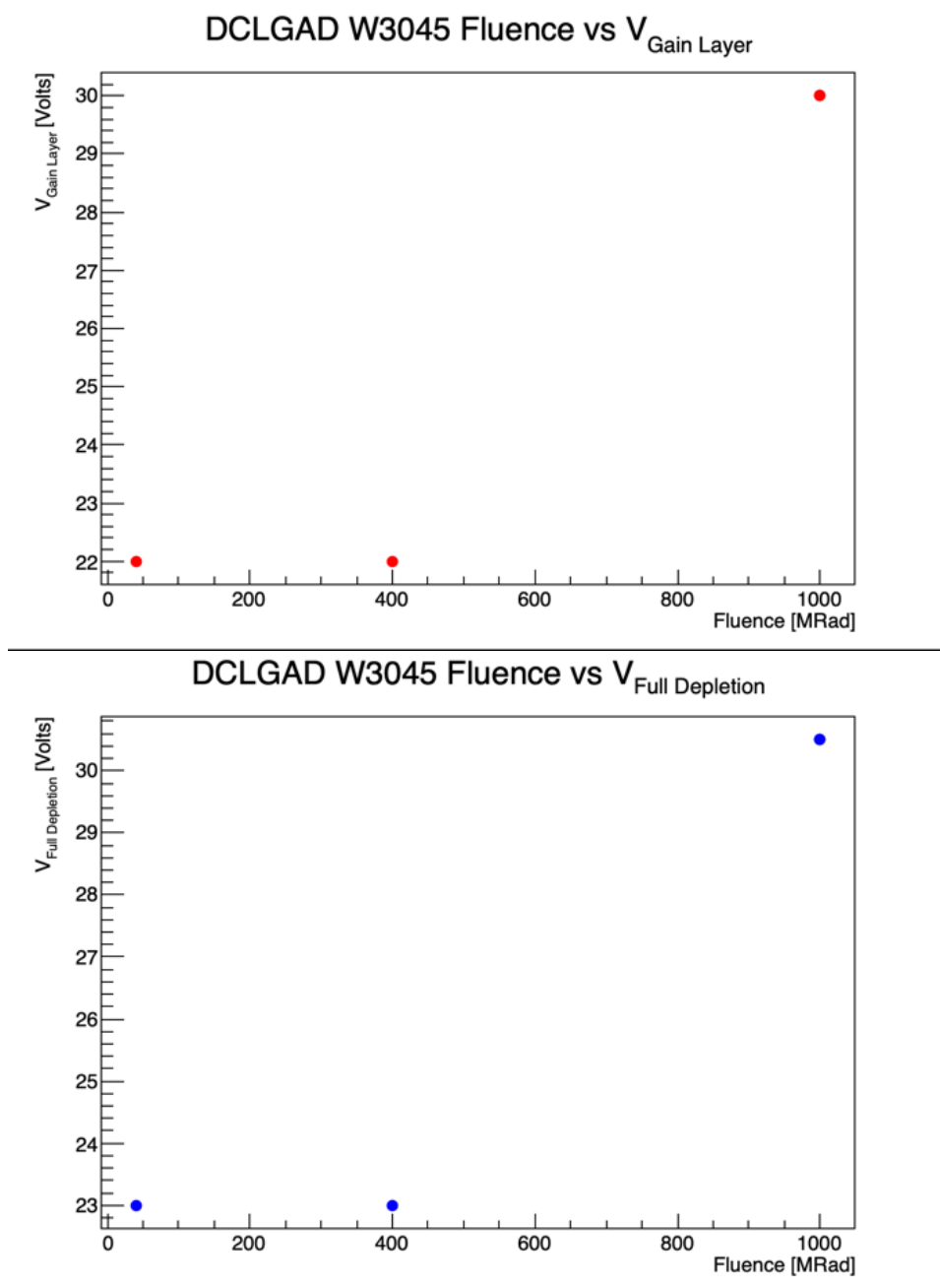


Figure 4.3: (Upper) gain layer depletion voltage versus fluence, and (Lower) full depletion voltage versus fluence for DC-LGAD detectors.

4.3.1 AC-LGADs

Figure 4.4 shows the gain layer depletion voltage versus fluence, and the full depletion voltage versus fluence for pixel AC-LGADs. Figure 4.5 shows the gain layer depletion voltage versus fluence, and the full depletion voltage versus fluence for strip AC-LGADs.

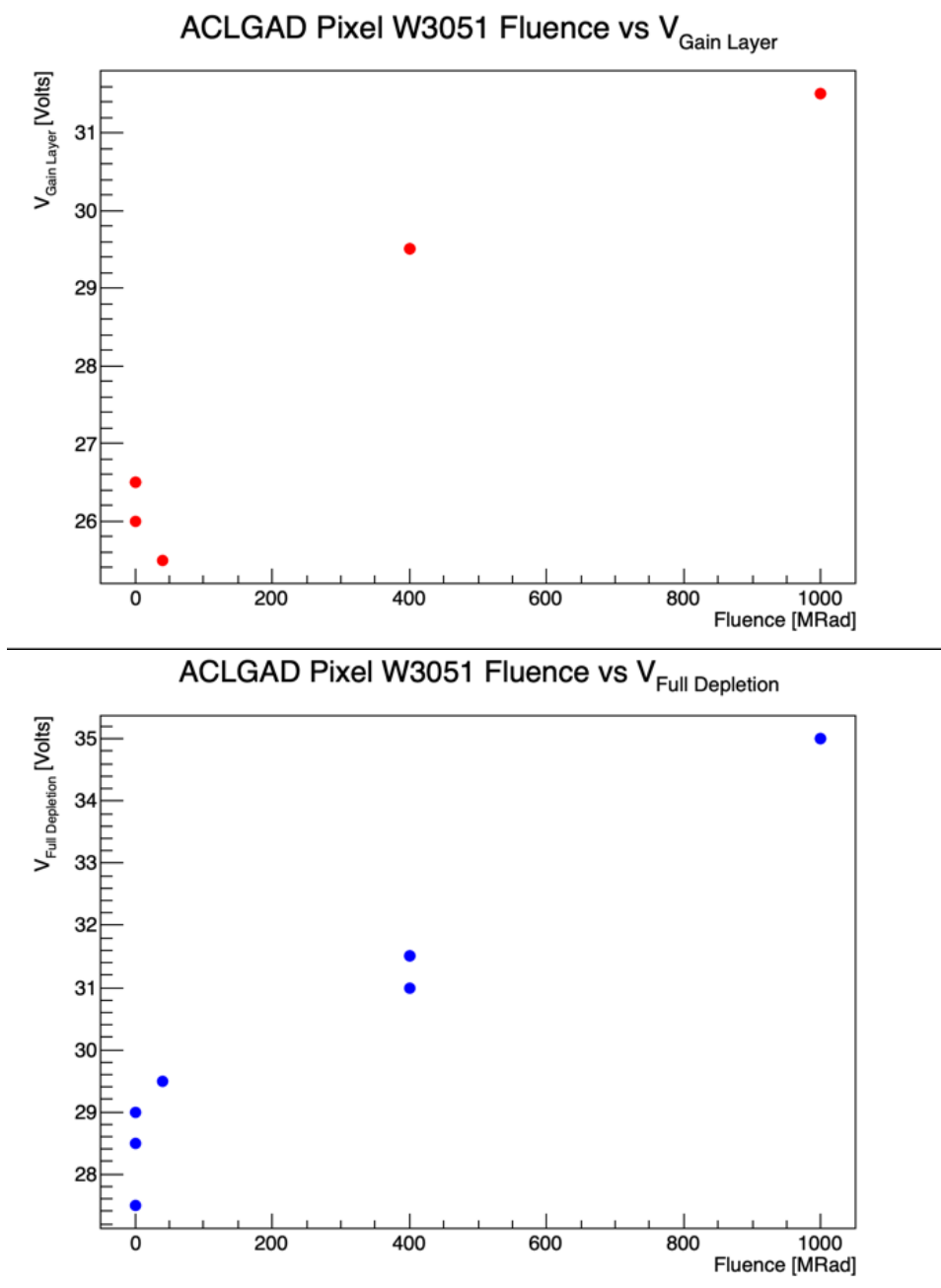


Figure 4.4: (Upper) gain layer depletion voltage versus fluence, and (Lower) full depletion voltage versus fluence for AC-LGAD pixel detectors.

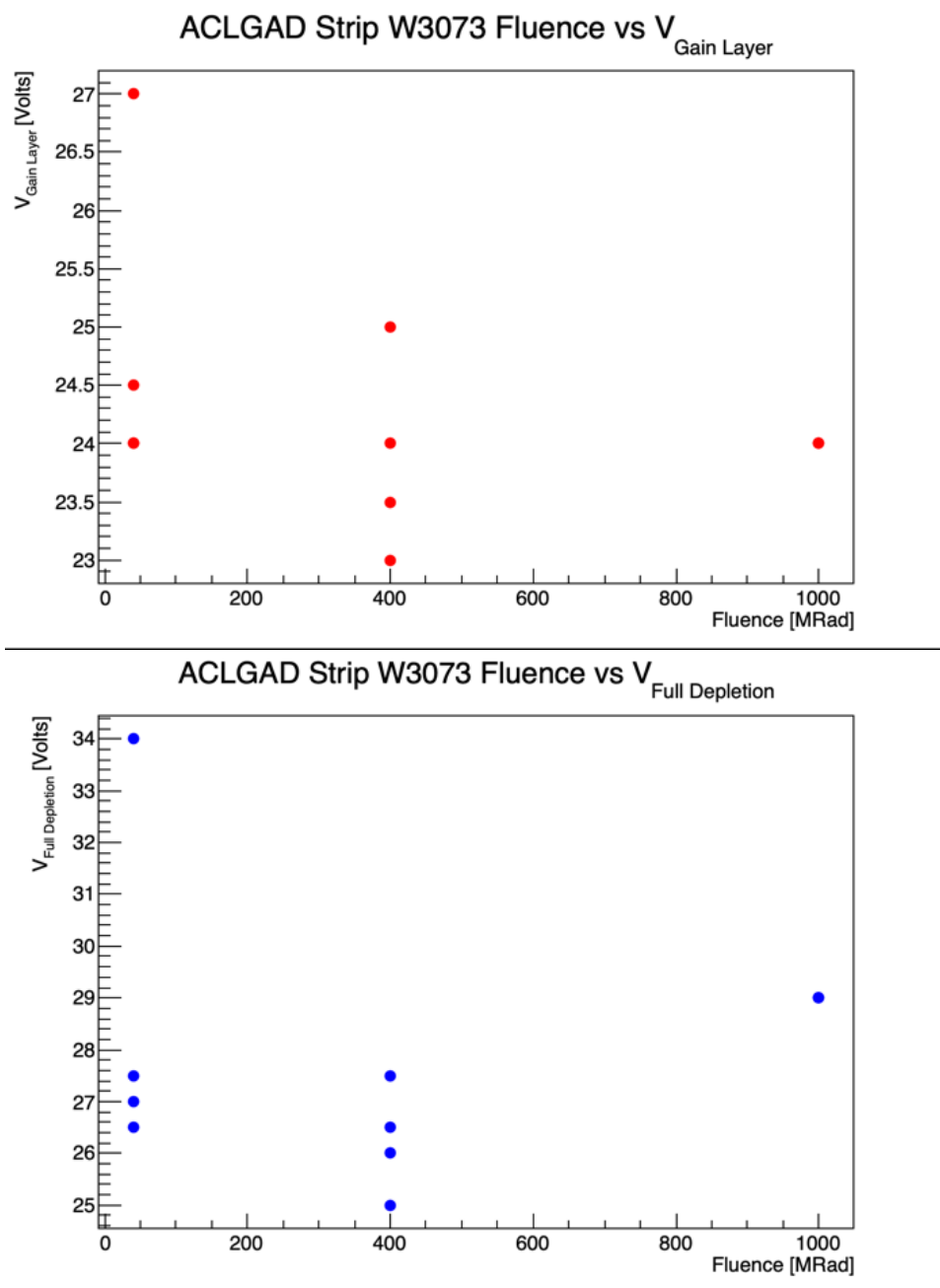


Figure 4.5: (Upper) gain layer depletion voltage versus fluence, and (Lower) full depletion voltage versus fluence for AC-LGAD strip detectors.

4.3.2 BNL DC-LGADs

Figures 4.6, 4.7, and 4.8 show properties of unirradiated BNL DC-LGAD sensors. Figure 4.6 shows the results of the measured potential, V , at which the gain layer is depleted of free charges. Figure 4.7 shows the results of the measured potential, V , at which the sensor is fully depleted of free charges. Figure 4.8 shows the results of the measured potential, V , at which breakdown occurs.

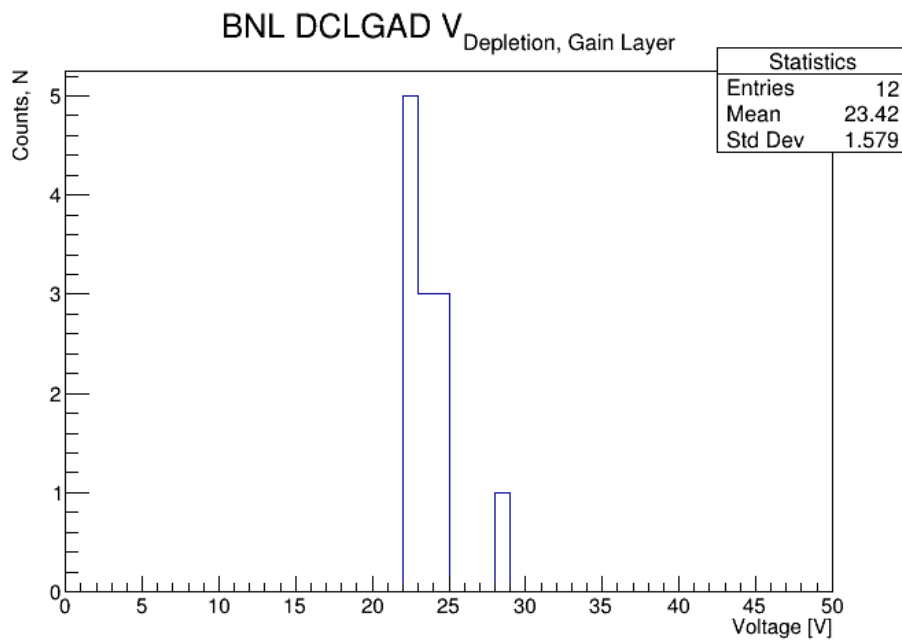


Figure 4.6: Distribution of measured potential, V , at which the gain layer is depleted of free charges for BNL DC-LGADs.

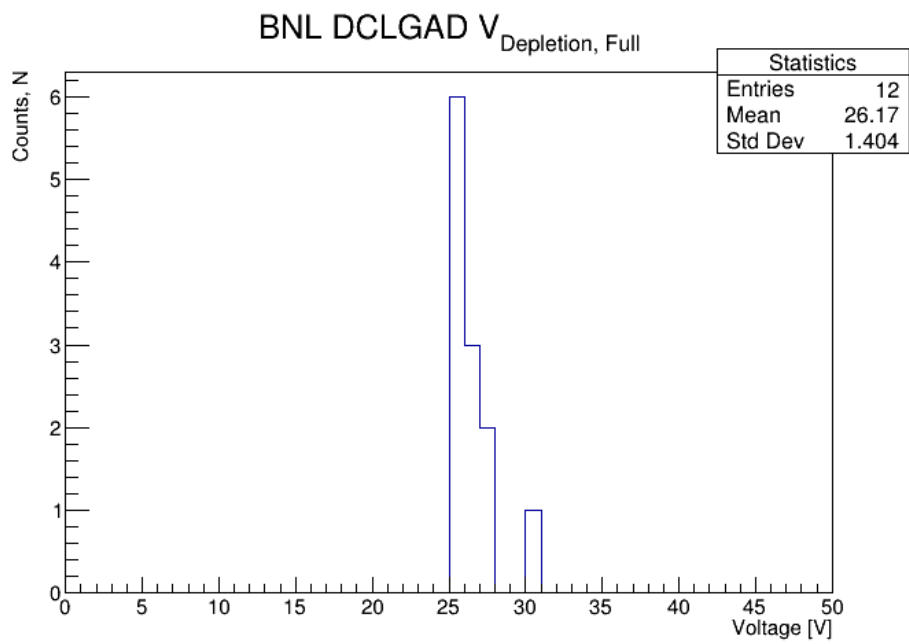


Figure 4.7: Distribution of measured potential, V , at which the sensor is fully depleted of free charges for BNL DC-LGADs.

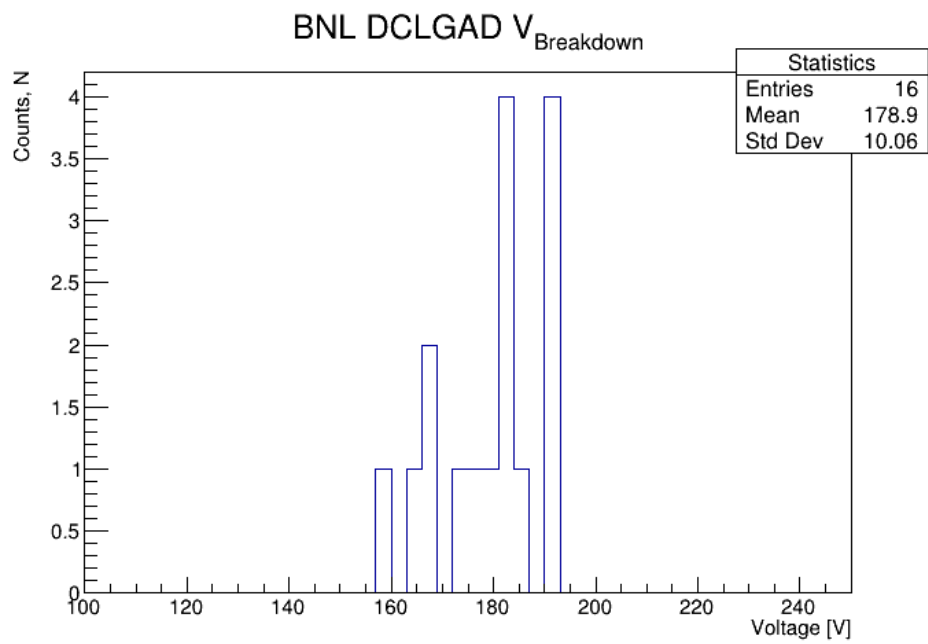


Figure 4.8: Distribution of measured potential, V , at which breakdown occurs for BNL DC-LGADs.

Chapter 5

Conclusion

I have successfully determined the operational ranges for many 3D sensors by using the depletion and breakdown voltage. I have also confirmed an increase in breakdown voltage and leakage current with temperature for 3D sensors. I have found that the Depletion Voltage is shown to increase with fluence. I have determined the operational ranges for many LGADs by measuring their breakdown and depletion voltage by measuring the leakage current. In doing this I gained the ability to find the same properties for other sensors.

Chapter 6

Acknowledgment

I would like to thank the Rayburn Reaching Up Fund for funding undergraduate research such as this, and the National Science Foundation for funding Research Experience for Undergraduates.

Thank you as well to my research advisors Sally Seidel and Jiahe Si, for supporting and developing my research. Thank you to Joey Sorenson, Radek Novotny, Easwar Narayanan, Hijas Farook, and Andrew Gentry for their generous help and support.

Bibliography

- [1] Da Vià, C., *Radiation Sensors with 3D Electrodes*, 1st ed., CRC Press, Taylor & Francis Group, 2019.
- [2] Ferrero, M., et al., *An Introduction to Ultra-Fast Silicon Detectors*, 1st ed., CRC Press, Taylor & Francis Group, 2021.
- [3] Giacomini, G., et al., *Fabrication and performance of AC-coupled LGADs* JINST 14 P09004, 2019.
- [4] Giacomini G., “LGAD-Based Silicon Sensors for 4D Detectors,” *Sensors*. 23, 2132. <https://doi.org/10.3390/s23042132>, 2023.
- [5] Hoferkamp, M., et al., *Characterization of Low Gain Avalanche Detector Prototypes’ Response to Gamma Radiation*, *Front. Phys.*, 10:838463, 2022.
- [6] McDuff, H., et al., “The effect of humidity on reverse breakdown in 3D silicon sensors,” *Nuclear Instruments and Methods in Physics Research Section A: Accelerators, Spectrometers, Detectors and Associated Equipment*, 785, 1-4, 2015.
- [7] Neaman, D., *Semiconductor Physics and Devices Basic Principles*, 4th ed., McGraw Hill, 2012.

- [8] Obertino M., “Performance of CMS 3D silicon pixel detectors before and after irradiation” *Nuclear Instruments and Methods in Physics Research Section A: Accelerators, Spectrometers, Detectors and Associated Equipment*, 730 33-37, 2013.
- [9] Pellegrini, G., et al., *Technology developments and first measurements of Low Gain Avalanche Detectors (LGAD) for high energy physics applications*, Nucl. Instr. and Meth. A 765 12, 2014.
- [10] Sadrozinski, H., et al., Ultra-fast Silicon Detectors, Nucl. Instr. and Meth. A 730 226, 2013.
- [11] Sorenson., J., et al., *Investigation of low gain avalanche detectors exposed to proton fluences beyond $10^{15} \text{n}_{eq} \text{cm}^{-2}$* , arXiv:2311.02027 [physics.ins-det], 2023.
- [12] Sze, S.M., “Physics of Semiconductor Devices,” 2nd Ed., Wiley, 1984.